J Mater Sci: Mater Electron (2013) 24:230–238
DOI 10.1007/s10854-012-0722-9

Investigation of indentation size effect (ISE) and micro-mechanical properties of Lu added $Bi_2Sr_2CaCu_2O_y$ ceramic superconductors

O. Ozturk · M. Erdem · E. Asikuzun · O. Yildiz · G. Yildirim · A. Varilci · C. Terzioglu

Received: 30 January 2012 / Accepted: 6 April 2012 / Published online: 22 April 2012

Abstract In this study, we investigated the effect of the Lutetium (Lu) addition on microstructure and mechanical properties of the *Bi-2212* superconductors annealed at 840 °C for 50 h. The samples were prepared by the widely used conventional solid-state reaction method. For comparison, undoped sample was prepared in the same conditions. The prepared samples were characterized using X-ray powder diffraction (XRD), scanning electron microscope (SEM), and microhardness measurements (H_v). The volume fraction and lattice parameters were determined from the *XRD* measurements. The microstructure, surface morphology and orientation of the grains were investigated by *SEM*. In this study we have focused on microhardness measurements to investigate the mechanical properties. Vickers microhardness, load independent hardness, Young's modulus, fracture toughness and yield strength values were calculated separately for doped and undoped samples. Experimental results of hardness measurements were analyzed using the Meyer's law, proportional sample resistance (*PSR*)model, modified proportional sample resistance (*MPRS*) model, Elastic–Plastic deformation model (*EPD*), and Hays-Kendall (*HK*) approach. Finally, the Hays-Kendall (*HK*) approach was determined as the most successful model describing the mechanical properties of our samples. Moreover, lattice parameter *c* and volume fraction of *Bi-2212* phase decreased with increasing *Lu* content. *SEM* measurements show that not only the surface morphology and grain connectivity were obtained to degrade but also the grain sizes of the samples were found to decrease with the increase of the *Lu* addition, as well.

O. Ozturk (✉) · E. Asikuzun · O. Yildiz
Department of Physics Faculty of Arts and Science, Kastamonu University, 37100 Kastamonu, Turkey
e-mail: oozturk@kastamonu.edu.tr

M. Erdem · G. Yildirim · A. Varilci · C. Terzioglu
Department of Physics Faculty of Arts and Science, Abant Izzet Baysal University, 14280 Bolu, Turkey

1 Introduction

The mechanical properties of high temperature superconductors are as important as the superconducting properties like critical temperature, critical current density, and critical magnetic field for industrial applications in the form of wires and tapes.

The superconducting wires and tapes are prone to mechanical stress when they are wound to form coils. Under mechanical stress, micro cracks form and thus the critical current density and critical magnetic field decrease abruptly. Therefore, investigation of the mechanical properties of superconductors is important for practical applications [1–4]. Indentation hardness testing is a generally used technique for investigation of mechanical properties of materials. The principle of indentation hardness testing is composed of application of load to the indenter and forming an indentation on the surface of the material. The hardness is calculated using the sizes of the formed indentation. Indentation hardness test is nondestructive since it produces only a small indention on the surface of the material.

Hardness is related to the structure and composition of materials, therefore it is a popular method to characterize materials [5]. Three properties of materials are effective in indentation; (1) the crystal structure of the grains, (2) grain orientation, (3) porosity among grains [6]. Hardness is a measure of porosity. Smaller values of hardness are obtained where porosity is high [7]. Therefore, the results of the hardness values must be endorsed by *XRD* and *SEM* measurements.

In this study, Vickers microhardness measurements are made to investigate the mechanical properties of Lutetium added *Bi-2212* superconducting samples prepared by solid state reaction method. *XRD* measurements are made to analyze lattice parameters and phase composition, and *SEM* measurements are used to analyze surface structure and grain orientation. The results of these measurements are used to analyze the mechanical properties using various models on *Lu* added *Bi-2212* superconductor.

2 Experimental details

Conventional solid state reaction method is used to prepare the *Lu* added *Bi-2212* samples. Lu_2O_3 (Alfa Aesar Co., Ltd., 99.9 % purity) powder is added to *Bi-2212* superconductor powder in the ratios of 0.1 % (Lu0.1), 0.3 % (Lu0.3), 0.5 (Lu0.5), 0.7 % (Lu0.7), and 1.0 % (Lu1.0). The resultant powders are mixed for 5 h to obtain homogeneity. The obtained powders are pressed into tablets of 13 mm diameter and 1–1.5 mm thickness under at 10 tons. Then the tablets are sintered at 840 °C for 50 h with 5 °C/min heating and 3 °C/min cooling rates. In addition to the *Lu* added samples, an undoped sample is produced using the same conditions to make comparison.

Vickers microhardness measurements are made at room temperature using Shimadzu HVM-2 digital microhardness tester. The load (F), was applied for 10 s in the range 0.245–2.940 N. The indenter was pressed on to different parts of the surface of the samples making sure that the indentations do not overlap. Vickers microhardness values are calculated and various hardness models are analyzed. In addition, the phase compositions are characterized by *XRD* investigation by Bruker D8 Advance *XRD* with CuK_α radiation ($\lambda = 1.5418$ Å) in the range $2\theta = 5$–60° at a scan speed of 3°/min and a step increment of 0.02° at room temperature. Phase ratio and lattice parameters a and c are determined from the *XRD* patterns. The accuracy in determining the lattice parameters (a and c) is determined to be ±0.0001 Å. Additionally, the average particle sizes of the samples produced are computed with the aid of the Scherrer–Warren approach. Moreover, the grain size, grain connectivity and surface morphology of the samples are identified using a Jeol scanning electron microscope (SEM) JEOL 6390-LV, operated at 20 kV, with a resolution power of 3 nm.

3 Result and discussion

3.1 XRD analysis

The XRD peaks of the Lu0.0, Lu0.3, Lu0.5, and Lu1.0 samples are shown in Fig. 1. As can be seen from the Fig. 1, all the

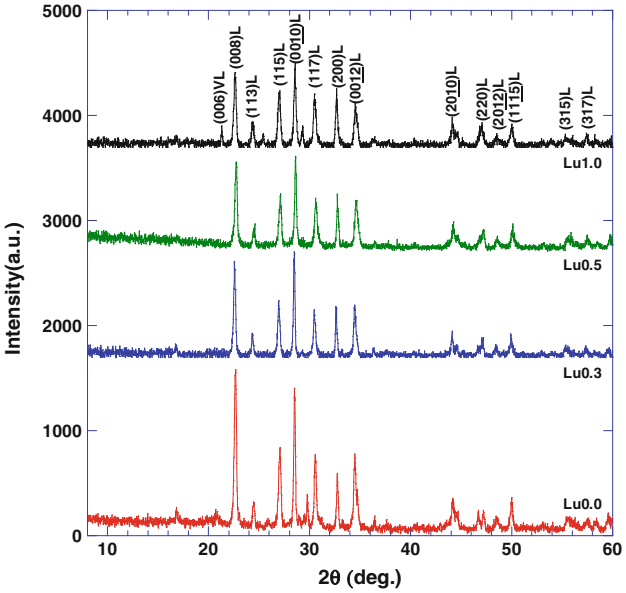

Fig. 1 *XRD* patterns of the Lu0.0, Lu0.3, Lu0.5 and Lu1.0 samples

samples studied exhibit the polycrystalline superconducting phase. The intensities of peaks belonging to (Bi, Pb)-2212 phase are obtained to decrease and the 2201-phase volume fraction increases with the increase in the Lu addition. But the dominant phase is the *Bi-2212* phase. The variation of a and c lattice parameters and volume fraction of phases with *Lu* addition are tabulated in Table 1. With the increase in *Lu* addition, a parameter initially increases and then decreases after a maximum, but the c parameter monotically decreases (Fig. 2). The change in the c parameter is due to settling of added rare earth elements into the crystal structure of *Bi-2212* superconductor [8–10]. When +3 valency rare earth ions substitute +2 valency Sr or Ca ions, one electron is added to the crystal structure. This addition of extra electron to the crystal structure causes an increase in oxygen content. This excess oxygen is captured by oxygen deficient *Bi–O* double planes. The positive charge in *Bi–O* planes decreases resulting in a decrease of the repelling force among positive charges, the binding between the planes increases. The distance between the *Bi–O* double planes and the c parameter decrease [11, 12]. Another possible explanation of c parameter contraction is due to the small ionic radius of *Lu.* Since *Lu* has the smallest ionic radius among lanthanides, replacement of Ca^{+2} or Sr^{+2} by Lu^{+3} ions causes the c parameter to decrease.

3.2 Grain size calculation

Using *XRD* analysis, the grain sizes can be calculated. The following equation is used to estimate the average grain sizes (Scherrer–Warren equation):

Table 1 *XRD* and resistivity measurement results for the samples

Samples	a (Å)	c (Å)	Volume fraction (%)		Grain size (Å)
			2212	2201	
Lu0.0	5.38	30.67	85	15	5.032
Lu0.1	5.39	30.64	68	32	4.611
Lu0.3	5.40	30.45	65	35	3.765
Lu0.5	5.39	30.21	64	36	3.717
Lu0.7	5.37	30.01	62	38	3.236
Lu1.0	5.35	29.59	59	41	3.164

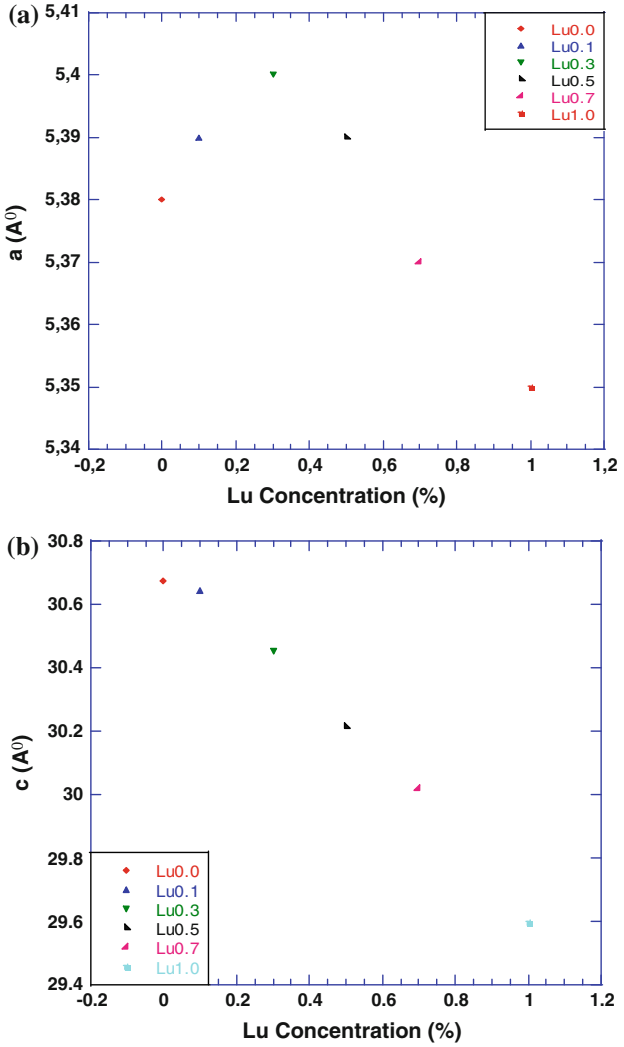

Fig. 2 Variation of lattice parameter as a function of *Lu* concentration

$$D = 0.941\lambda/\beta\cos\theta_\beta \quad (1)$$

Where D is grain size, λ is the wavelength of X-ray, β is FWHM (full width at half maximum) of the peak with the highest intensity, and θ is the angle of the peak. The results of the calculated grain sizes are tabulated in Table 1. From the table it can be seen that the grain sizes decrease with *Lu* addition. This result is compatible with our *SEM* results.

3.3 SEM analysis

To analyze the surface structure, to detect possible precipitations in the grain boundaries, and to estimate the grain sizes of the samples *SEM* images are used. Figure 3 shows the surface images of Lu0.0 and Lu1.0 samples. The images show that addition of *Lu* changed the surface morphologies of the samples. Grain sizes and grain orientation decrease with *Lu* addition and the porosity increases. Figure 3 shows that the pure sample without *Lu* addition is denser and has lower porosity than the *Lu* added sample. According to *SEM* results, the surface morphology, grain connectivity and average crystallite size are found to degrade with increasing *Lu* addition, which is supported by grain size calculation results.

3.4 Microhardness and modelling

After application of different loads, Vickers microhardness values are calculated using the following equation

$$H_v = 1854.4\left(F/d^2\right) \quad \text{(GPa)} \quad (2)$$

The calculated results of load dependent H_v, E, $Y$and K_{IC} are given in Table 2.

Figure 4 shows the change in Vickers microhardness as a function of the applied load. The figure shows that the microhardness increases monotically with increasing *Lu* content. It can be seen that for all samples, the microhardness values are load dependent—a phenomenon known as *ISE* (Indentation Size Effect). The microhardness values of all samples are higher at lower applied loads, but they decrease as the applied load is increased. The hardness-load curve shows a transition to a plateau for higher values of applied load. The plateau values of microhardness are argued to correspond to the load independent (intrinsic) microhardness values [13]. Since microhardness changes with applied load, the real value of microhardness is

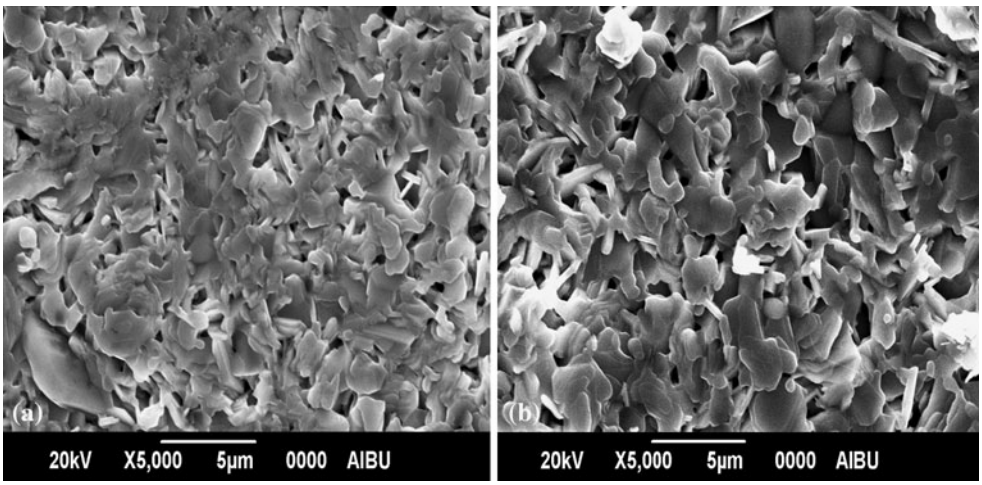

Fig. 3 *SEM* micrographs of **a** Lu0.0 and **b** Lu1.0 samples

Table 2 The calculated load dependent H_v, E, Y and K_{IC} for the samples

Samples	Load (N)	H_v (GPa)	E (GPa)	Y (GPa)	K_{IC} (Pam$^{-1/2}$)
Lu0.0	0.245	0.986	80.81	0.328	955.62
	0.490	0.810	66.39	0.270	881.34
	0.980	0.715	58.60	0.238	813.76
	1.960	0.622	50.98	0.207	759.00
	2.940	0.593	48.60	0.197	741.09
Lu0.1	0.245	1.094	89.66	0.364	1,024.26
	0.490	0.878	71.96	0.292	917.58
	0.980	0.790	64.75	0.263	870.39
	1.960	0.717	58.76	0.239	829.20
	2.940	0.681	55.81	0.227	808.12
Lu0.3	0.245	1.242	101.79	0.414	952.91
	0.490	1.068	87.53	0.356	883.64
	0.980	1.027	84.17	0.342	866.51
	1.960	0.951	77.94	0.317	833.83
	2.940	0.910	74.58	0.303	815.66
Lu0.5	0.245	1.433	117.45	0.477	1,104.05
	0.490	1.213	99.42	0.404	966.72
	0.980	1.154	74.58	0.384	942.92
	1.960	1.032	84.58	0.344	891.68
	2.940	0.979	80.24	0.326	868.48
Lu0.7	0.245	1.587	130.07	0.529	1,274.07
	0.490	1.374	112.61	0.458	1,185.48
	0.980	1.235	101.22	0.411	1,123.93
	1.960	1.110	90.97	0.370	1,065.55
	2.940	1.052	86.22	0.350	1,037.34
Lu1.0	0.245	1.687	138.27	0.562	1,342.77
	0.490	1.455	119.25	0.485	1,247.00
	0.980	1.312	107.53	0.437	1,184.14
	1.960	1.220	99.99	0.406	1,141.87
	2.940	1.163	95.32	0.387	1,114.90

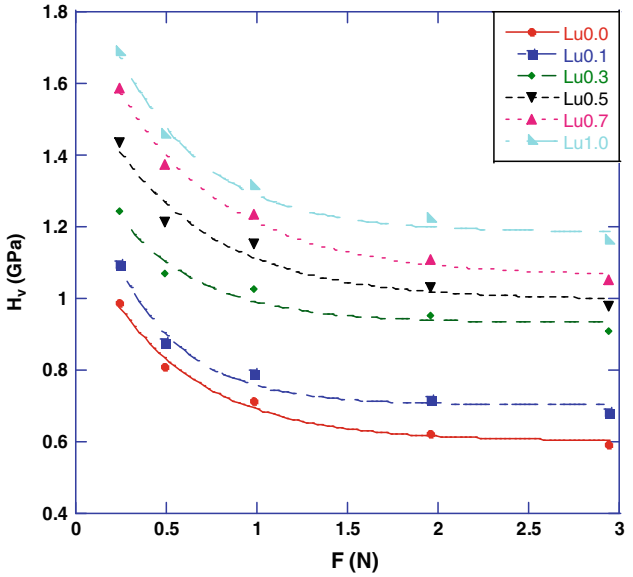

Fig. 4 Variation of load dependent microhardness H_v with applied load F

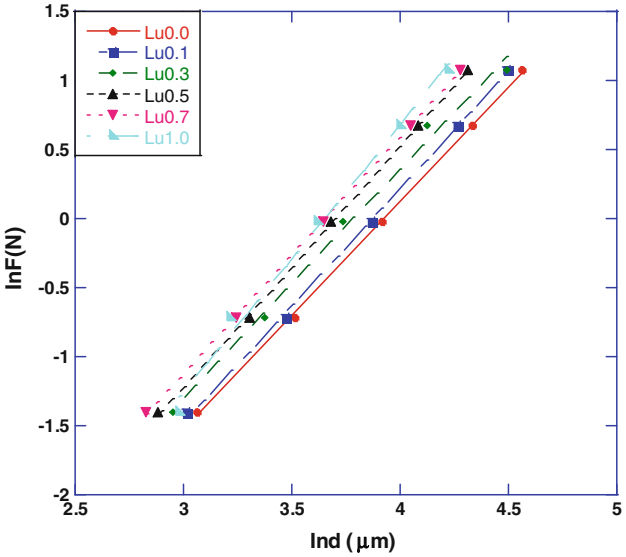

Fig. 5 Variation of applied load *lnF* with diagonal *lnd* for the samples

ambiguous. In literature, various models are proposed to explain *ISE* behaviour. In this study, Meyer's law, Hays-Kendall approach (HK), Proportional sample resistance (PSR) model, Modified proportional sample resistance (MPSR) model, and elastic/plastic deformation (EPD) model are used to analyze microhardness results of our samples.

3.4.1 Analysis according to Meyer's law

Meyer's law is a generally used model to explain *ISE*. This law is a simple expression between applied load F and indentation depth d:

$$F = Ad^n \tag{3}$$

where n is Meyer number which is calculated from the fitted curves of experimental data. Meyer number n is a measure of *ISE* for values of n higher than 2, *ISE* behaviour is not observed [13–15].

The slope of the graph in Fig. 5 gives n_k, and the vertical intercept is A_{1K}. For all of our samples, Meyer number is less than 2 which proves that load dependent displacement has *ISE* behaviour. The results obtained from the graph are tabulated in Table 3.

3.4.2 Analysis according to PSR model

Another model to analyze *ISE* behaviour is proportional sample resistance (PSR) model. Li and Bradt reported that PSR model is suitable to explain *ISE* behaviour in various materials [16]. The following expression is used in this model:

$$F = \alpha d + \beta d^2 \tag{4}$$

where α gives the surface energy, and β gives load independent hardness value. The values of α and β are calculated from the F/d versus d graph of Fig. 6. The change in α is associated with the energy distribution of the surface cracks [17].

The load independent microhardness value according to *PSR* model is calculated using;

$$H_{PSR} = 1854.4\beta \tag{5}$$

From Table 4 it is seen that the values of α are positive for all samples. This result shows that there is elastic deformation in the samples along with plastic deformation.

Equations (6–8) and load independent H_{PSR} is used to calculate load independent elastic modulus (E_0), tensile stress (Y_0), and fracture toughness (K_{IC}) values which are tabulated in Table 5. H_0, E_0 and Y_0 values increase with *Lu* concentration. This is an expected result since microhardness increases with Lu concentration. The increase in K_{IC} is related to the increase in α the surface energy. Fracture

Table 3 Best-fit results of experimental data according to Meyer's law

Samples	n_k	In A_{1K} (GPa)
Lu0.0	1.660	−6.520
Lu0.1	1.689	−6.534
Lu0.3	1.656	−6.265
Lu0.5	1.743	−6.447
Lu0.7	1.717	−6.276
Lu1.0	1.931	−7.046

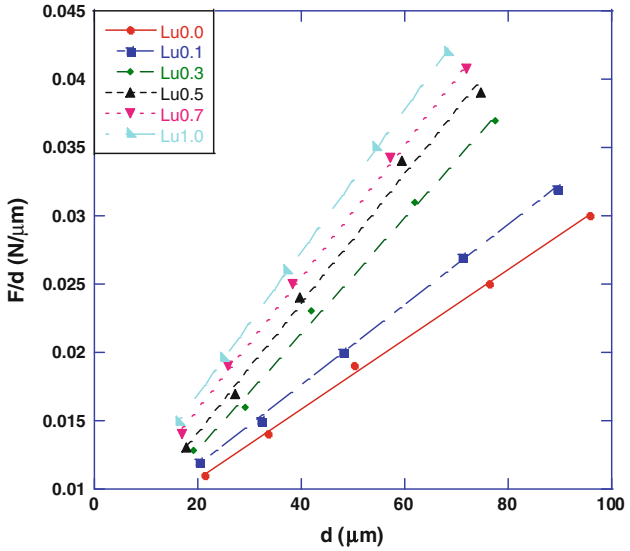

Fig. 6 Plots of *F/d* versus *d* for the samples

toughness (K_{IC}) is an important parameter for technological applications.

$$E = 81.9635H_v \tag{6}$$

$$Y \approx H_v/3 \tag{7}$$

$$K_{ic} = \sqrt{2E\gamma} \tag{8}$$

3.4.3 Analysis according to modified PSR (MPSR) model

According to *PSR* model, when $d = 0$ the resistance of the sample ($W = A_1 d$) becomes zero [18, 19]. That means the minimum amount of applied load needed permanent deformation is zero. Gong et al. [19] proposed that the sample subject to mechanical treatments like surface polishing can be considered as a compressed spring rather than a relaxed one. *MPSR* model is defined with the following equation;

$$F = W_{MPSR} + A_{0MPSR}d + A_{1MPSR}d^2 \tag{9}$$

The load independent microhardness value due to *MPSR* model can be calculated using;

$$H_{MPSR} = 1854.4A_{1MPSR} \tag{10}$$

The values W_{MPSR} and A_{MPSR} calculated from fitting of the curve in Fig. 7 and the associated load independent microhardness values are given in Table 6. From the table it can be seen that the microhardness values calculated using the *MPSR* model are far from the values of the plateau region.

3.4.4 Analysis according to elastic/plastic deformation (EPD) model

According to Bull et al. [20, 21], the dependence of indentation size on the applied load is given as;

$$F = A_2(d_p + d_e)^2 \tag{11}$$

where A_2 is a constant, and d_e is related to d_p plastic deformation. The values of A_2 and d_e can be calculated from $F^{1/2}$ versus d graph (Fig. 8).

The load independent microhardness due to this model is calculated as;

Table 4 Best-fit results of experimental data according to *PSR* model

Samples	$\alpha \times 10^{-3}$ (N)	$\beta \times 10^{-5}$ (N/μm)	Load independent hardness H_{PSR} (GPa)	Load dependent hardness H_v (GPa)
Lu0.0	5.65	25.46	0.472	0.593–0.622
Lu0.1	5.85	29.37	0.544	0.681–0.717
Lu0.3	4.46	42.45	0.787	0.910–0.951
Lu0.5	4.70	47.29	0.877	0.979–1.032
Lu0.7	6.24	48.43	0.898	1.052–1.110
Lu1.0	6.52	52.00	0.964	1.163–1.220

Table 5 The calculated load independent H_0, E_0, Y_0 and K_{IC} for the samples

Samples	H_0 (GPa)	E_0 (GPa)	Y_0 (GPa)	K_{ic} (Pa/m$^{1/2}$)	H_v (GPa)
Lu0.0	0.472	38.686	0.157	661.17	0.593–0.622
Lu0.1	0.544	44.588	0.181	213.68	0.681–0.717
Lu0.3	0.787	64.505	0.262	758.54	0.910–0.951
Lu0.5	0.877	71.881	0.292	675.68	0.979–1.032
Lu0.7	0.898	73.603	0.299	958.41	1.052–1.110
Lu1.0	0.964	79.012	0.321	1,015.04	1.163–1.220

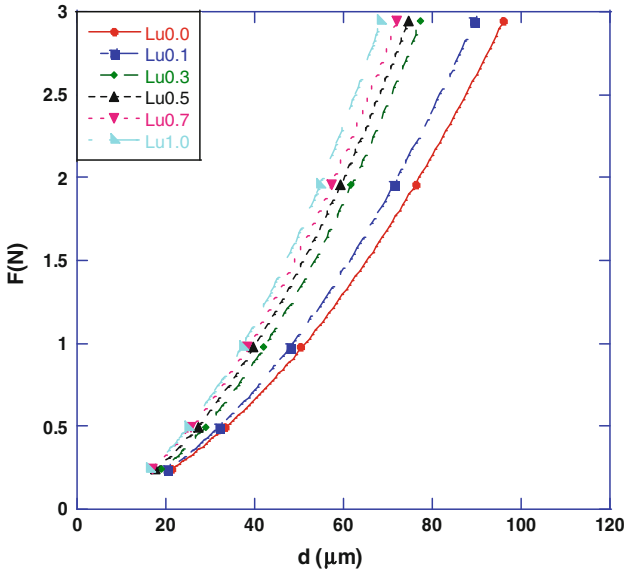

Fig. 7 Variation of applied load with the indentation diagonal length for the samples

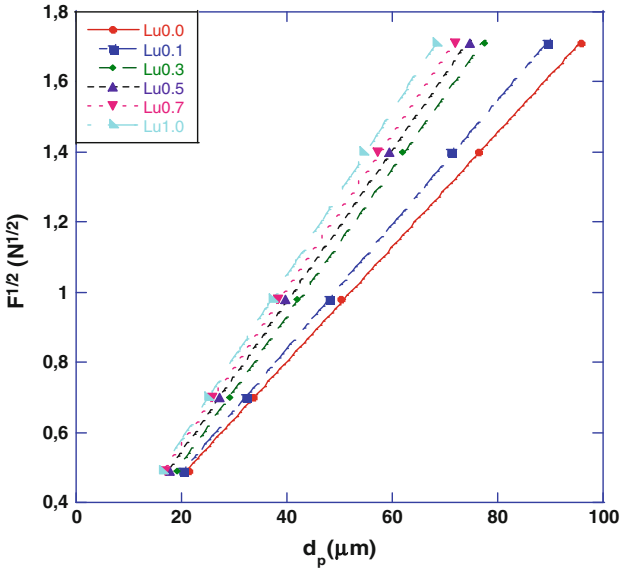

Fig. 8 Plots of diagonal length versus square root of applied loads for the samples

$$H_{EPD} = 1854.4A_2 \tag{12}$$

As seen from Table 7, the value of d_e is positive for all samples. That means for this range of applied loads elastic deformation is observed along with plastic deformation. For all samples elastic relaxation is present. Presence of elastic deformation along with plastic deformation is the reason of *ISE* behaviour for our samples.

3.4.5 Analysis using Hays-Kendall approach

Hays–Kendall [22] reported that in the microhardness measurements of various materials, only elastic deformation is observed for applied loads less than a critical value, but above the critical value plastic deformation is observed. Gane and Bowden [23] observed that for various materials, the indenter does not penetrate into the sample until the applied load reaches a critical value and then abruptly penetrates into the sample for applied loads above this critical value. Moreover, although the applied load increases the size of the indentation does not increase until the applied load reaches the critical value. Hays-Kendall suggested that the indentation size is related to an effective load $F_{eff} = F - W_{HK}$ rather than the applied load itself.

$$F - W_{HK} = A_{1HK}d^2 \tag{13}$$

where A_1 is a load independent constant. The values of W_{HK} and $A_{1HK}$are calculated from F versus d^2 graph (Fig. 9). The curves are linear for all samples. The slope of the graph in Fig. 9 gives the value of A_{1HK}. The load independent microhardness value due to this model is;

$$H_{HK} = 1854.4A_{1HK} \tag{14}$$

In Table 8, the values of W_{HK}, A_{1HK} and the load independent microhardness values are tabulated. The values of W_{HK} are positive for all samples which can be interpreted as the applied load is enough to create both the elastic and plastic deformation [24].

For all samples exhibiting *ISE* behaviour, among the models used the values of microhardness calculated using HK model are the closest to the values of the plateau

Table 6 Best-fit results of experimental data according to *MPSR* model

Samples	W_{MPRS} (N)	$A_{0MPRS} \times 10^{-5}$ (N/μm)	$A_{1MPRS} \times 10^{-5}$ (N/μm^2)	Load independent hardness H_{MPRS} (GPa)	H_v (GPa)
Lu0.0	−0.025	734.6	24.555	0.455	0.593–0.622
Lu0.1	−0.019	663.42	29.600	0.548	0.681–0.717
Lu0.3	−0.058	769.39	40.185	0.745	0.910–0.951
Lu0.5	−0.077	1,041.8	40.259	0.746	0.979–1.032
Lu0.7	−0.056	1,024.8	43.617	0.808	1.052–1.110
Lu1.0	−0.031	815.27	51.594	0.956	1.163–1.220

Table 7 Best-fit results of experimental data according to *EPD* model

Samples	H_{EPD} (GPa)	d_e (μm)	H_v (GPa)
Lu0.0	0.492	0.148	0.593–0.622
Lu0.1	0.580	0.130	0.681–0.717
Lu0.3	0.817	0.090	0.910–0.951
Lu0.5	0.857	0.113	0.979–1.032
Lu0.7	0.905	0.125	1.052–1.110
Lu1.0	0.980	0.109	1.163–1.220

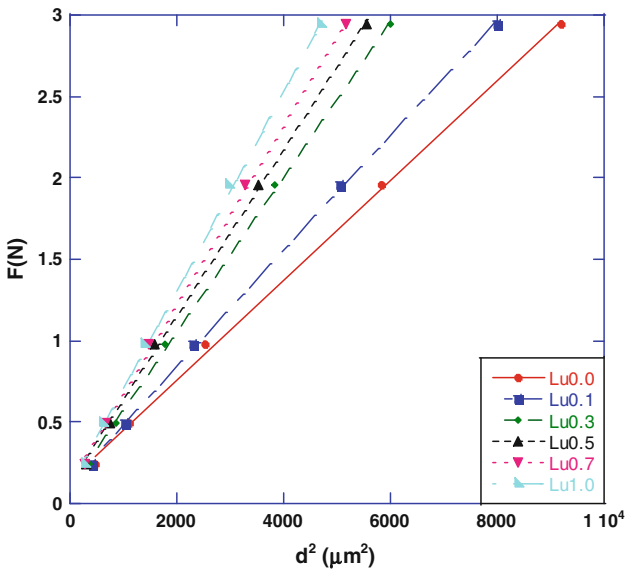

Fig. 9 Applied load versus the square of the impression semi-diagonal length for the samples

(saturation) region (Table 9). In literature it is indicated that the load independent microhardness values should be close to the values of the plateau region [19, 25–27]. Therefore, Hays–Kendall model is more suitable to determine the micromechanical properties and *ISE* behavior of our samples.

4 Conclusion

The effects of *Lu* addition on the mechanical and superconducting properties of *Bi-2212* superconductors are studied in detail. To determine the mechanical properties, Vickers microhardness measurements are made. The results of the microhardness measurements are analyzed using Meyer's law, *PSR*, *MPRS*, *EPD,* and Hays-Kendall *(HK)* approach. The following results are obtained;

- The *XRD* analysis showed that the *a* lattice parameter and *Bi-2201* phase ratio increased slightly, but *c* lattice parameter and *Bi-2212* phase ratio decreased with *Lu* addition. No other detectable phases are obtained which indicate that majority of *Lu* ions settle into the crystal structure.
- The *SEM* results indicate that the grain sizes decrease; the grain connectivities and the surface structure deteriorate with *Lu* addition. The decrease in grain sizes is endorsed with the grain size calculations of the *XRD* peaks.
- Vickers microhardness values increase with *Lu* addition. This result seems to be incompatible with our SEM analysis since the grain connectivity and texturing decrease and porosity increases with *Lu* addition. We argue that a possible explanation is as follows: *Lu* itself has a high value of microhardness. Actually *Lu* has the highest hardness and density among lanthanides. Settling of *Lu* in the intergranular spacing and interfaces of the samples increases the microhardness of the *Lu* added samples. Lu addition can also suppress microcracking and thus improve the mechanical connections among the grains.
- Elastic modulus, tensile stress, and fracture toughness values for both load dependent and load independent case increase with addition.
- The results of the microhardness measurements are analyzed employing Meyer's law, *PSR*, *MPSR*, *EDP* models and Hays–Kendall approach. Hays–Kendall approach is found to be the best model describing the microhardness of our samples.

Table 8 Best-fit results of experimental data according to *HK* model

Samples	A_{1HK}	W_{HK} (N)	Load independent hardness H_{HK} (GPa)	H_v (GPa)
Lu0.0	30.631×10^{-5}	0.149	0.568	0.593–0.622
Lu0.1	35.455×10^{-5}	0.130	0.657	0.681–0.717
Lu0.3	47.925×10^{-5}	0.096	0.888	0.910–0.951
Lu0.5	51.196×10^{-5}	0.122	0.949	0.979–1.032
Lu0.7	54.819×10^{-5}	0.130	1.016	1.052–1.110
Lu1.0	60.931×10^{-5}	0.111	1.127	1.163–1.220

Table 9 The results of load dependent Vickers microhardness at the plateau region and load independent hardness values calculated using *PSR*, *MPSR*, *EPD* and *HK* models

Samples	H_v (GPa) (in plateau region)	H_{PSR} (GPa)	H_{MPSR} (GPa)	H_{EPD} (GPa)	H_{HK} (GPa)
Lu0.0	0.593–0.622	0.472	0.455	0.492	0.568
Lu0.1	0.681–0.717	0.544	0.548	0.580	0.657
Lu0.3	0.910–0.951	0.787	0.745	0.817	0.888
Lu0.5	0.979–1.032	0.877	0.746	0.857	0.949
Lu0.7	1.052–1.110	0.898	0.808	0.905	1.016
Lu1.0	1.163–1.220	0.964	0.956	0.980	1.127

References

1. S.X. Dou, H.K. Liu, Supercond. Sci. Technol. **6**, 297–314 (1993)
2. S.M. Khalil, J. Phys. Chem. Solids **64**, 855 (2003)
3. C. Terzioglu, M. Yilmazlar, O. Ozturk, E. Yanmaz, Phys. C **423**, 119–126 (2005)
4. M. Yilmazlar, H.A. Cetinkara, M. Nursoy, O. Ozturk, C. Terzioglu, Phys. C **442**, 101–107 (2006)
5. O. Uzun, U. Kölemen, S. Çelebi, N. Güçlü, J. Eur. Ceram. Soc. **25**(6), 969–977 (2005)
6. U. Kölemen, S. Çelebi, H. Karal, A. Öztürk, U. Çevik, S. Nezir, O. Görür, Phys. Stat. Sol. B. **241**, 274–283 (2004)
7. E. Asikuzun, O. Ozturk, H.A. Cetinkara, G. Yildirim, A. Varilci, M. Yılmazlar, C. Terzioglu, J. Mater. Sci. Mater. Electron. (2011). doi:10.1007/s10854-011-0537-0
8. S. Vinu, P.M. Sarun, A. Biju, R. Shabna, P. Guruswamy, U. Syamaprasad, Supercond. Sci. Technol. **21**, 045001 (2008)
9. R. Shabna, P.M. Sarun, S. Vinu, A. Biju, U. Syamaprasad, Supercond. Sci. Technol. **22**, 045016 (2009)
10. A. Varilci, M. Altunbas, O. Gorur, I. Karaca, S. Celebi, Phys. Status Solidi A **194**, 206 (2002)
11. S. Vinu, P.M. Sarun, R. Shabna, A. Biju, U. Syamaprasad, Mater. Lett. **62**, 4421–4424 (2008)
12. M. Okada, Supercond. Sci. Technol. **13**, 29 (2000)
13. J.B. Quinn, V.D. Quinn, J. Sci. **32**, 4331–4346 (1997)
14. H.A. Cetinkara, M. Yilmazlar, O. Ozturk, M. Nursoy, C. Terzioglu, J. Phys. Conf. Ser. **153**, 012038 (2009)
15. O. Ozturk, E. Asikuzun, M. Erdem, G. Yildirim, O. Yildiz, C. Terzioglu, J. Mater. Sci. Mater. Electron. (2011). doi:10.1007/s10854-011-0429-3
16. H. Li, R.C. Bradt, J. Mater. Sci. **28**, 917–926 (1993)
17. A. Leenders, M. Mich, H.C. Freyhard, Phys. C **279**, 173 (1997)
18. U. Kölemen, O. Uzun, M. Yılmazlar, N. Güçlü, E. Yanmaz, J. Alloy. Compd. **415**, 300–306 (2006)
19. J. Gong, J. Wu, Z. Guan, Mater. Lett. **38**, 197 (1999)
20. G.P. Upit, S.A. Varchenya, Phys. Status Solidi A **17**, 831 (1966)
21. S.J. Bull, T.F. Page, E.H. Yoffe, Philos. Mag. Lett. **59**, 281 (1989)
22. C. Hays, E.G. Kendall, Metallography **6**, 275–282 (1973)
23. N. Gane, J. Appl. Phys. **39**, 1432–1435 (1968)
24. R. Awad, A.I. Abou-Aly, M. Kamal, M. Anas, J. Supercond. Nov. Magn. **24**, 1947–1956 (2011)
25. J. Gong, Z. Zhao, Z. Guan, H. Mıao, J. Eur. Ceram. Soc. **20**, 1895–1900 (2000)
26. Z. Peng, J. Gong, H. Mıao, J. Eur. Ceram. Soc. **24**, 2193–2201 (2004)
27. O. Ozturk, H.A. Cetinkara, E. Asıkuzun, M. Akdogan, M. Yilmazlar, C. Terzioglu, J. Mater. Sci. Mater. Electron. **22**, 1501–1508 (2011)